International Journal of Multiphase Flow 34 (2008) 819–828

Contents lists available at ScienceDirect

International Journal of Multiphase Flow

journal homepage: www.elsevier.com/locate/ijmulflow

Turbulent particle dispersion in arbitrary wall-bounded geometries: A coupled CFD-Langevin-equation based approach

A. Dehbi *

Paul Scherrer Institut, Department of Nuclear Energy and Safety, Laboratory for Thermal-hydraulics, 5232 Villigen PSI, Switzerland

ARTICLE INFO

Article history:
Received 21 December 2007
Received in revised form 10 March 2008
Available online 15 March 2008

Keywords:
Continuous random walk
Langevin equation
Inhomogeneous turbulence
Wall-bounded flows
CFD
DNS

ABSTRACT

A Lagrangian continuous random walk (CRW) model is developed to predict turbulent particle dispersion in arbitrary wall-bounded flows with prevailing anisotropic, inhomogeneous turbulence. The particle tracking model uses 3D mean flow data obtained from the Fluent CFD code, as well as Eulerian statistics of instantaneous quantities computed from DNS databases. The turbulent fluid velocities at the current time step are related to those of the previous time step through a Markov chain based on the normalized Langevin equation which takes into account turbulence inhomogeneities. The model includes a drift velocity correction that considerably reduces unphysical features common in random walk models. It is shown that the model satisfies the well-mixed criterion such that tracer particles retain approximately uniform concentrations when introduced uniformly in the domain, while their deposition velocity is vanishingly small, as it should be. To handle arbitrary geometries, it is assumed that the velocity rms values in the boundary layer can locally be approximated by the DNS data of fully developed channel flows. Benchmarks of the model are performed against particle deposition data in turbulent pipe flows, 90° bends, as well as more complex 3D flows inside a mouth-throat geometry. Good agreement with the data is obtained across the range of particle inertia.

1. Introduction

Turbulent flows which transport particulates are quite often encountered in a vast array of environmental, industrial, and medical applications. Examples of particle-laden flows can be found in atmospheric dispersion of pollutants, sediment transport in rivers, drug delivery in human airways, fouling in compressor and turbine blades, chemical pulping, nuclear fission products transport, etc. Hence, an accurate description of particle transport is of great practical importance. While particle transport in isotropic and homogeneous turbulent fields has been extensively studied (Yeung and Pope, 1989; Squires and Eaton, 1991), wall-bounded flows have not comparatively attracted the same attention. In the latter, boundary layers form close to the walls, and turbulence is strongly anisotropic and inhomogeneous, which renders the problem quite a bit more complicated. Of particular importance in boundary layer flows is the understanding of mechanisms responsible for particle preferential concentration (Marchioli and Soldati, 2002), which in turn explain many macroscopic features such as the particle deposition rates on the walls. The heart of the particle dispersion problem resides in modeling the random velocity fluctuations which particles encounter along their trajectories.

As summarized by Dehbi (2008), one can distinguish two main families of methods to treat particle dispersion in fluid flows: Eulerian and Lagrangian. In the Eulerean or "two-fluid" approach, the particles are regarded as a continuous phase for which the averaged conservation equations (continuity, momentum and energy) are solved in similar fashion to the carrier gas flow field (Zhang and Prosperetti, 1994). The Eulerean approach is particularly suitable for denser suspensions when particle–particle interactions are important and the particle feedback on the flow is too large to ignore. The main challenge facing Eulerian-type, two-fluid approaches resides in accurately defining the inter-phase exchange rates and closure laws which arise from the averaging procedures (Drew, 1983). In addition, the strong coupling between the phases renders the Eulerean approach quite delicate to handle, especially at boundaries where the solid phase may be removed or reflected.

The Lagrangian approach (Maxey, 1987) treats particles as a discrete phase which is dispersed in the continuous phase. The particle volume loading is usually assumed negligible, so that particles have no feedback effect on the carrier gas and particle–particle interactions are neglected. In the Lagrangian framework, the controlling phenomena for particle dispersion in the field are assessed using a rigorous treatment of the forces acting on the particle. In general, the detailed flow field is computed first, then a representatively large number of particles are injected in the domain, and their trajectories determined by following individual particles until

* Tel.: +41 56 310 27 11; fax: +41 310 27 99.
E-mail address: abdel.dehbi@psi.ch

0301-9322/$ - see front matter © 2008 Elsevier Ltd. All rights reserved.
doi:10.1016/j.ijmultiphaseflow.2008.03.001

they are removed from the gas stream or leave the computational space. Particle motion is extracted from the time integration of Newton's second law, in which all the relevant forces can be incorporated (drag, gravity, lift, thermophoretic force, etc.). The Lagrangian approach is computationally intensive, because it entails tracking a large number of particles until stationary statistics are achieved. On the other hand, the results of Lagrangian particle tracking (LPT) are physically easier to interpret. Therefore, in the following investigation, the LPT methodology is used, along with the assumption that the dispersed phase is dilute enough not to affect the continuous flow field (one-way coupling).

Many methods have been developed to take into account velocity fluctuations in the turbulent flow. In principle, the simplest and more "physical" method is Direct Numerical Simulation (DNS) (McLaughlin, 1989) in which turbulence is "reproduced" by solving the transient Navier–Stokes continuity and momentum equations on a sufficiently fine grid and with a sufficiently small time step. In such a way, all relevant spatial and temporal scaled are resolved. Large-Eddy Simulations (LES) (Wang and Squires, 1997) are conceptually similar to DNS, except that the computational effort is reduced somewhat by requiring the grid to be only so fine as to resolve the largest eddies, whereas the smaller, quasi isotropic eddies are modeled. While being widely used, DNS-LES/LPT methods remain computationally expensive, and their extension to general geometries poses very tough and sometimes intractable computational challenges.

An alternative method, which borrows from the family of stochastic models, attempts to simulate turbulence using complementary equations whereby the instantaneous turbulent velocities are calculated from local quantities such as the mean turbulent kinetic energy, the Eulerian time scale and the distance to the wall. Examples of these treatments are random walk models which have been popular due to their relative ease of implementation and reasonable computational expense.

In Discrete Random Walk (DRW) models (Gosman and Ioannides, 1983), the turbulent dispersion of particles is modeled as a succession of interactions between a particle and eddies which have finite lengths and lifetimes. It is assumed that at time t_0, a particle with velocity U_p is captured by an eddy which moves with a velocity composed of the mean fluid velocity, augmented by a random "instantaneous" component which is piecewise constant in time. When the lifetime of the eddy is over or the particle crosses the eddy, another interaction is generated with a different eddy, and so forth. In wall-bounded flows, the original isotropic DRW model of Gosman and Ioannides (1983) has been improved to account for anisotropic turbulence in the near-wall regions. This improved DRW model has been used with some success to predict turbulent particle deposition in isothermal 2D channels (Kallio and Reeks, 1989), in general 3D isothermal flows (Dehbi, 2008) or in cooled pipes (Kröger and Drossinos, 2000).

Continuous Random Walk (CRW) models provide a more physically sound picture of fluid turbulence, as they represent the instantaneous velocities in a continuous way. CRW models, which are usually based on the Langevin equation, have been shown to provide more realistic predictions of turbulent particle dispersion than DRW, in particular in flows where inhomogeneous effects are important such as mixing layers (MacInnes and Bracco, 1992) or free shear flows (Bocksell and Loth, 2001). Hence a CRW model will be adopted in this investigation.

One of the main goals of this investigation is to describe turbulent particle dispersion in general wall-bounded geometries. Mean flow parameters in complex turbulent flows can only be predicted on a routine basis using standard Computational Fluid Dynamics (CFD) tools based on the Reynolds Averaged Navier Stokes (RANS) equations. Ideally then, turbulent particle dispersion in general 3D geometries could be done by coupling CFD with reliable particle dispersion models in a single application. However, as shown recently by Tian and Ahmadi (2007), the use e.g. of DRW in combination with the state-of-the-art anisotropic Reynolds Stress Model (RSM) still led to large overpredictions of particle deposition rates in 2D parallel ducts. This is due to the fact that the RSM calculated root mean square (rms) of the normal velocity near the wall overpredicts the profiles determined by DNS studies, and no grid refinement can remedy this problem. Using the same RSM-DRW framework, Parker et al. (in press) were able to obtain dimensionless deposition velocities that overestimated the experimental data by less than one order of magnitude, which is the best that can be achieved with today's CFD codes in their default mode. Better results were however obtained when Tian and Ahmadi (2007) combined the use of RSM for the mean flow field, the Langevin equation for the turbulent fluctuations, and a DNS-supplied correlation for the normal velocity rms close to the wall.

Based on the above, it becomes clear that quantitatively accurate predictions of turbulent particle dispersion in general 3D geometries can only be achieved through a substantial improvement in the treatment of particle-turbulence interactions in the boundary layer. This treatment needs to be developed and incorporated in the CFD tools in order to properly account for near-wall effects which control to a large extent the physics of particle deposition. In this investigation, the fluid fluctuations will be computed from a Langevin equation based model, which will be combined with the mean flow data obtained from the Fluent 6.3 code (Fluent, 2006). Fluent 6.3 is a state of the art code based on finite volume methods that provides a wide choice of turbulence models (k–ε, k–ω, RSM, etc). The necessary Eulerian statistics to close the Lagrangian particle tracking model will be supplied by the available DNS databases of channel flows.

2. Particle equations of motion

Let a spherical particle be entrained in a turbulent flow. Assuming only drag and gravity are significant, the vector force balance on that particle is written as follows:

$$\frac{dU_p}{dt} = F_D(U - U_p) + g\left(1 - \frac{\rho_f}{\rho_p}\right) \tag{1}$$

where the drag force per unit mass may be expressed as

$$F_D = \frac{18\mu}{\rho_p d_p^2} C_D \frac{Re_p}{24} \tag{2}$$

In the above, U is the fluid velocity, U_p is the particle velocity, ρ_p the particle density, ρ_f the fluid density, g the gravity acceleration vector, d_p the particle geometric diameter, μ the fluid molecular viscosity, and Re_p the particle Reynolds number defined as

$$Re_p = \frac{d_p \mid U - U_p \mid}{\nu} \tag{3}$$

ν being the fluid kinematic viscosity. The drag coefficient is computed in the Fluent code from the following equation:

$$C_D = \beta_1 + \frac{\beta_2}{Re_p} + \frac{\beta_3}{Re_p^2} \tag{4}$$

where the β's are constants which apply to spherical particles for wide ranges of Re_p. The trajectory $x(x_1,x_2,x_3,t)$ of the particle is obtained by integration of the following velocity vector equation with respect to time:

$$U_p = \frac{dx}{dt} \tag{5}$$

The expressions (1)–(5) are all one needs to compute the trajectory of individual particles in laminar flows. The particle concentration

and deposition are deduced in a determinist way, and the procedure was shown by Healy and Young (2001) to accurately predict particle dispersion. When turbulence is present in the flow, the computation of particle dispersion becomes significantly more involved as the random velocity fluctuations do not allow for a deterministic knowledge of particle trajectories. One then resorts to stochastic computations of a great many trajectories with the aim to capture "average" particle dispersion. The CRW describing the model for velocity history is introduced next.

3. The conventional Langevin equation and drift correction

The time history of carrier fluid fluctuations a particle sees as it moves in a flow dictates to a large extend its dispersion and deposition characteristics in turbulent fields. In homogenous turbulence, one of the most common ways to describe fluid velocity fluctuations in a continuous way is through the so-called Langevin equation. This equation was proposed by Langevin in the early 1900's to model the random Brownian motion of very small particles. The change in the particle velocity with time is assumed to be comprised of a damping term which is proportional to velocity, and a random forcing term that has zero mean. Obukhov (1959) extended this concept to fluid velocity fields in homogeneous turbulence, and in this context, the Langevin equation becomes a stochastic differential equation which uses Markov chains to specify a possible increment du_i in the fluid velocity fluctuation:

$$\mathrm{d}u_i = -u_i(t)\frac{\mathrm{d}t}{\tau_i} + \sigma_i\sqrt{\frac{2}{\tau_i}}\cdot \mathrm{d}\xi_i \tag{6}$$

The incremental displacement $\mathrm{d}x_i$ during a time $\mathrm{d}t$ is thus:

$$\mathrm{d}x_i = (U_i + u_i)\mathrm{d}t \tag{7}$$

In the above, τ_i is a timescale, σ_i the fluctuating rms of velocity $\sqrt{\overline{u_i^2}}$, x_i the ith coordinate, and $d\xi_i$ a succession of uncorrelated random numbers with zero mean and variance $\mathrm{d}t$. It is usual to assume the ξ_i distribution to be Gaussian, which will be the case in this investigation.

As stressed by Iliopoulos and Hanratty (1999), the Langevin equation is not exact and only comparison with experiments or DNS results will allow one to conclude to its usefulness.

The Langevin equation was extensively used to model homogeneous turbulence where the rms values and Lagrangian time scales are position independent. In wall-bounded flow, however, turbulence is strongly inhomogeneous and anisotropic in the boundary layer, which implies some modification of the Langevin equation is in order.

Several authors have attempted to take turbulent inhomogeneity into account. For instance, Legg and Raupach (1982) proposed that the wall-normal velocity fluctuations a fluid particle sees in the boundary layer be governed by the following equation for steady-state fully developed channel flows:

$$\mathrm{d}u_2 = -u_2\frac{\mathrm{d}t}{\tau_2} + \sigma_2\sqrt{\frac{2}{\tau_2}}\cdot \mathrm{d}\xi_2 + \frac{\partial\sigma_2^2}{\partial x_2}\cdot \mathrm{d}t \tag{8}$$

In such a treatment, the last term is added as a mean drift correction that ensures that tracer-like particles will, on average, follow streamlines in inhomogeneous flows. In DRW or CRW simulations, the non-inclusion of this correction term results in non-physical diffusion of tracer particles with errors as high as 550% for simple flows, as shown by MacInnes and Bracco (1992), while its inclusion dramatically decreases the error for idealized inhomogeneous flows (Bocksell and Loth, 2001).

The correction for tracer particles can be shown to be necessary from the following simple analysis. Let us start from the instantaneous acceleration a_i of a fluid particle:

$$a_i = U_j\frac{\partial U_i}{\partial x_j} \tag{9}$$

where the Einstein convention of summing up over repeated indices is adopted. Expressing the instantaneous velocity as the sum of the mean and fluctuating parts, one writes

$$U_i = \overline{U_i} + u_i \tag{10}$$

where, by definition:

$$\overline{u_i} = 0 \tag{11}$$

The mean acceleration is obtained by inserting (10) in (9), and averaging over time while making use of (11). After algebraic manipulations, one gets

$$\bar{a}_i = \bar{a}_{i,\mathrm{mean}} + \bar{a}_{i,\mathrm{drift}} = \overline{U_j}\frac{\partial\overline{U_i}}{\partial x_j} + \overline{u_j\frac{\partial u_i}{\partial x_j}} \tag{12}$$

One can therefore break down the mean acceleration of a fluid particle into a component due to the mean flow, and a component due to random turbulent fluctuations in an inhomogeneous flow field. The drift acceleration gives rise then to a drift velocity that one needs to add in the Langevin equation to take into account turbulence inhomogeneities:

$$\delta u_i = \overline{u_j\frac{\partial u_i}{\partial x_j}}\cdot \mathrm{d}t = \frac{\partial\overline{u_iu_j}}{\partial x_j}\cdot \mathrm{d}t \tag{13}$$

To arrive at the second equality in (13), it is necessary to assume a divergence-free fluctuating velocity field, which is reasonable for the incompressible flows addressed in this investigation. The form taken by the correction depends on the particular flow conditions. In the wall-normal direction of the boundary layer, the fully-developed assumption results in the wall-normal derivative of $\sigma_2^2 = \overline{u_2u_2}$ to be dominant in the right hand side of Eq. (13), hence the form of the drift correction in the conventional Langevin equation (8).

The drift correction velocity as expressed in (13) is in principle applicable only to tracer particles which perfectly follow the fluid fluctuations. Perkins (1992) and later Pozorski and Minier (1998) suggested adjusting the Lagrangian time scale τ_i to account for the fact that inertial particles do not exactly follow the fluid streamlines. A simpler approach was followed by Iliopoulos et al. (2003) who assumed that the fluid velocity seen by inertial particles is the same as that seen by fluid particles, and hence the drift correction in (13) applies to inertial particles as well to a first approximation. A more rigorous analysis was performed by Bocksell and Loth (2006) who derived a drift correction that applies to particles with arbitrary inertia. Using the instantaneous acceleration of a fluid particle along the path of an inertial particle, Bocksell and Loth (2006) showed that the drift correction for an inertial particle can be obtained from the drift correction of a fluid particle through a multiplicative factor as follows:

$$\delta u_i = \frac{\partial\overline{u_iu_j}}{\partial x_j}\cdot\left(\frac{1}{1+Stk}\right)\cdot \mathrm{d}t \tag{14}$$

where the particle Stokes number is defined as

$$Stk = \frac{\tau_\mathrm{p}}{\tau_\mathrm{L}} \tag{15}$$

In the above, τ_L is a Lagrangian time scale to be specified later in Section 6, and τ_p the particle relaxation time defined according to the prevailing particle Reynolds number:

$$\tau_\mathrm{p} = \frac{C_\mathrm{c}\rho_\mathrm{p}d_\mathrm{p}^2}{18\mu}, \quad Re_\mathrm{p} \leqslant 1 \tag{16}$$

and

$$\tau_\mathrm{p} = \frac{4}{3}\frac{\rho_\mathrm{p}}{\rho_\mathrm{f}}\frac{C_\mathrm{c}d_\mathrm{p}^2}{C_\mathrm{D}\mid U-U_\mathrm{p}\mid}, \quad Re_\mathrm{p} > 1 \tag{17}$$

C_c is the Cunningham correction slip factor which is very close to one for particles with diameters above 1 μm. Eq. (14) is valid provided the particle gravitational settling velocity is much smaller than the fluid velocity fluctuations (Bocksell and Loth, 2006).

From (14), one notes that the inertial particle drift correction behaves correctly at the extremes, i.e. for very large Stokes numbers, the fluctuating flow field and particle motion are decoupled, hence the drift correction tends to zero, whereas for non-inertial particles with Stokes number close to 0, the tracer correction limit holds and (14) reduces to (13).

4. The normalized Langevin equation in boundary layers

While providing better results in inhomogeneous flows than DRW models, the predictions of the CRW model based on the conventional Langevin equation (8) are not completely satisfactory (Bocksell and Loth, 2001). A significant step forward was made when Durbin (1983, 1984) and Thompson (1984), following the ideas of Wilson et al. (1981), proposed that the Langevin equation be normalized to account for inhomogeneous turbulence in the wall normal direction of a boundary layer. Following Iliopoulos et al. (2003), the normalized Langevin equation can thus be written as

$$\mathrm{d}\left(\frac{u_i}{\sigma_i}\right) = -\left(\frac{u_i}{\sigma_i}\right)\cdot\frac{\mathrm{d}t}{\tau_i} + \mathrm{d}\eta_i + A_i\mathrm{d}t \tag{18}$$

In the boundary layer, where the subscripts 1, 2 and 3 stand for streamwise, wall-normal and spanwise directions, respectively, one has

$$A_i = \frac{\partial\left(\frac{\overline{u_2u_i}}{\sigma_i}\right)}{\partial x_2} \tag{19}$$

while, to a first order, the forcing moments can be expressed as

$$\overline{\mathrm{d}\eta_i\mathrm{d}\eta_j} = \frac{\overline{u_iu_j}}{\sigma_i\sigma_j}\left[\frac{1}{\tau_i}+\frac{1}{\tau_j}\right]\cdot\mathrm{d}t \tag{20}$$

where overbar in the above expressions means time averages. Eq. (20) is obtained assuming jointly Gaussian distributions for the forcing terms η_i (Mito and Hanratty, 2002).

In the normalized Langevin equation (18), A_i is the mean drift correction term. In fact, for the wall normal direction, A_2 reduces to $\partial\sigma_2/\partial x_2$ and is the counterpart of the term $\partial\sigma_2^2/\partial x_2$ in the conventional Langevin equation (8), as demonstrated earlier by Wilson et al. (1981). Thompson (1987) showed that the inclusion the drift correction A_i fulfills the well-mixed criterion, i.e. that tracers which are initially well mixed in the inhomogeneous turbulent flow will remain well mixed. This was later also verified by Mito and Hanratty (2002) for fluid particles originating from uniformly distributed sources in channel flow boundary layers. Following Mito and Hanratty (2004), A_3 is set to zero.

From the preceding sections, the normalized Langevin equation with the inertial particle drift correction can be written as follows for the streamwise, normal, and spanwise directions of the boundary layer:

$$\mathrm{d}\left(\frac{u_1}{\sigma_1}\right) = -\left(\frac{u_1}{\sigma_1}\right)\cdot\frac{\mathrm{d}t}{\tau_1} + \sqrt{\frac{2}{\tau_1}}\cdot\mathrm{d}\xi_1 + \frac{\partial\left(\frac{\overline{u_1u_2}}{\sigma_1}\right)}{\partial x_2}\cdot\frac{\mathrm{d}t}{1+Stk} \tag{21}$$

$$\mathrm{d}\left(\frac{u_2}{\sigma_2}\right) = -\left(\frac{u_2}{\sigma_2}\right)\cdot\frac{\mathrm{d}t}{\tau_2} + \sqrt{\frac{2}{\tau_2}}\cdot\mathrm{d}\xi_2 + \frac{\partial\sigma_2}{\partial x_2}\cdot\frac{\mathrm{d}t}{1+Stk} \tag{22}$$

$$\mathrm{d}\left(\frac{u_3}{\sigma_3}\right) = -\left(\frac{u_3}{\sigma_3}\right)\cdot\frac{\mathrm{d}t}{\tau_3} + \sqrt{\frac{2}{\tau_3}}\cdot\mathrm{d}\xi_3 \tag{23}$$

where the timescales τ_i will be addressed later in Section 6.

5. The normalized Langevin equation in the isotropic bulk

In the bulk region, where turbulence is approximately isotropic, the Langevin equations remain of the same form for the damping and stochastic terms. However, a simpler formulation is required for the drift correction terms. Following Bocksell and Loth (2006), the normalized incremental drift correction along a particle path is expressed as follows:

$$\delta\left(\frac{u_i}{\sigma_i}\right) = \overline{u_j\frac{\partial\left(\frac{u_i}{\sigma_i}\right)}{\partial x_j}}\cdot\frac{\mathrm{d}t}{1+Stk} \tag{24}$$

Taking into account only the terms involving the normal stresses, and ignoring the cross terms in Eq. (24) as second order effects, one can show, with the help of the second equality in (13) that the drift correction reduces to

$$\delta\left(\frac{u_i}{\sigma_i}\right) = \overline{u_j\frac{\partial\left(\frac{u_i}{\sigma_i}\right)}{\partial x_j}}\cdot\frac{\mathrm{d}t}{1+Stk} \cong \frac{1}{2\sigma_i}\frac{\partial\sigma_i^2}{\partial x_i}\cdot\frac{\mathrm{d}t}{1+Stk} \tag{25}$$

Invoking isotropic turbulence in the bulk, one has

$$\sigma = \sigma_1 = \sigma_2 = \sigma_3 = \sqrt{\frac{2}{3}\cdot k} \tag{26}$$

Therefore, the drift correction in the isotropic bulk becomes

$$\delta\left(\frac{u_i}{\sigma_i}\right) = \overline{u_j\frac{\partial\left(\frac{u_i}{\sigma_i}\right)}{\partial x_j}}\cdot\frac{\mathrm{d}t}{1+Stk} \cong \frac{1}{3\sigma}\frac{\partial k}{\partial x_i}\cdot\frac{\mathrm{d}t}{1+Stk} \tag{27}$$

The turbulent kinetic energy k is readily available since it is one of the variables solved for by CFD codes.

In keeping up with the normalization of the Langevin equation, and adding the effect of particle inertia, one obtains the following equations for the bulk region with isotropic inhomogeneous turbulence:

$$\mathrm{d}\left(\frac{u_1}{\sigma}\right) = -\left(\frac{u_1}{\sigma}\right)\cdot\frac{\mathrm{d}t}{\tau_L} + \sqrt{\frac{2}{\tau_L}}\cdot\mathrm{d}\xi_1 + \frac{1}{3\sigma}\cdot\frac{\partial k}{\partial x_1}\cdot\frac{\mathrm{d}t}{1+Stk} \tag{28}$$

$$\mathrm{d}\left(\frac{u_2}{\sigma}\right) = -\left(\frac{u_2}{\sigma}\right)\cdot\frac{\mathrm{d}t}{\tau_L} + \sqrt{\frac{2}{\tau_L}}\cdot\mathrm{d}\xi_2 + \frac{1}{3\sigma}\cdot\frac{\partial k}{\partial x_2}\cdot\frac{\mathrm{d}t}{1+Stk} \tag{29}$$

$$\mathrm{d}\left(\frac{u_3}{\sigma}\right) = -\left(\frac{u_3}{\sigma}\right)\cdot\frac{\mathrm{d}t}{\tau_L} + \sqrt{\frac{2}{\tau_L}}\cdot\mathrm{d}\xi_3 + \frac{1}{3\sigma}\cdot\frac{\partial k}{\partial x_3}\cdot\frac{\mathrm{d}t}{1+Stk} \tag{30}$$

The timescales are τ_L are taken to be equal in all directions, in accordance with the isotropic turbulence assumption.

Eqs. (21)–(23) and (28)–(30) represent possible changes of the turbulent fluid velocities in the boundary layer and bulk region, respectively. The integration of these equations in time is done using the first order implicit Euler method, and the dynamic time step is taken to be min (10^{-6} s, $0.1\tau_p$), which was small enough not to affect the results. Hence, at each time step, $u(t+\Delta t)$ is obtained given $u(t)$. The integration of the equations requires the specification of the Lagrangain time scales and Eulerian statistics, which is done in the next sections.

6. Specification the time scales

The normalized Langevin equation as written in (18) allows for the spatial variation of σ_i and τ_i, i.e. inhomogeneous turbulence. As noted by Iliopoulos and Hanratty (1999), the time scale τ_i can be rigorously defined only in homogeneous turbulence. For inhomogeneous turbulence, some researchers estimate τ_i from the Eulerean spectra of fluctuating velocities, while others derive it from Lagrangian calculations, e.g., by tracking fluid particles in DNS simulations, and evaluating the Lagrangian autocorrelations. Bocksell and Loth (2006) have performed such computations in boundary

layer flows using 4000 tracer particles and concluded that their Lagrangian time scale correlations in all directions are comparable and reasonably well approximated by the fits provided by Kallio and Reeks (1989).

$$\tau_L^+ = 10, \quad y^+ \leqslant 5 \tag{31}$$

$$\tau_L^+ = 7.122 + 0.5731 \cdot y^+ - 0.00129 \cdot y^{+2}, \quad 5 \leqslant y^+ \leqslant 100 \tag{32}$$

where

$$\tau_L = \tau_L^+ \cdot \frac{v}{(u^*)^2} \tag{33}$$

In the above expression, y^+ is the wall distance in dimensionless units:

$$y^+ = \frac{yu^*}{v} \tag{34}$$

and u^* is the friction velocity at the wall defined by

$$u^* = \sqrt{\frac{\tau_w}{\rho_f}} \tag{35}$$

where τ_w is the local wall shear stress.

For simplicity, and following the findings of Bocksell and Loth (2006), it will be assumed hereafter that the boundary layer Lagrangian timescales in all 3 directions (τ_1,τ_2, τ_3) are all equal to τ_L.

Away from the boundary layer, i.e. in the bulk flow where $y^+ > 100$, the Lagrangian time scale can be calculated from the turbulent kinetic energy k and dissipation rate ε:

$$\tau_L = \frac{2}{C_o} \cdot \frac{k}{\varepsilon} \tag{36}$$

Mito and Hanratty (2002) concluded that away from the wall region, a value of 14 for C_0 provided good agreement with time scales computed from their DNS investigations. In the context of this work, k and ε are obtained from CFD computations of the mean flow field.

7. Specification of Eulerian statistics in the boundary layer

In the boundary layer, taken here to be the region for which $y^+ < 100$, the Eulerian rms of velocity are obtained from DNS fits of channel flow (Re = 13 000) obtained by Dreeben and Pope (1997):

$$\sigma_1^+ \equiv \frac{\sigma_1}{u^*} = \frac{0.40 \cdot y^+}{1 + 0.0239(y^+)^{1.496}} \tag{37}$$

$$\sigma_2^+ \equiv \frac{\sigma_2}{u^*} = \frac{0.0116 \cdot (y^+)^2}{1 + 0.203 \cdot y^+ + 0.00140(y^+)^{2.421}} \tag{38}$$

$$\sigma_3^+ \equiv \frac{\sigma_3}{u^*} = \frac{0.19 \cdot y^+}{1 + 0.0361(y^+)^{1.322}} \tag{39}$$

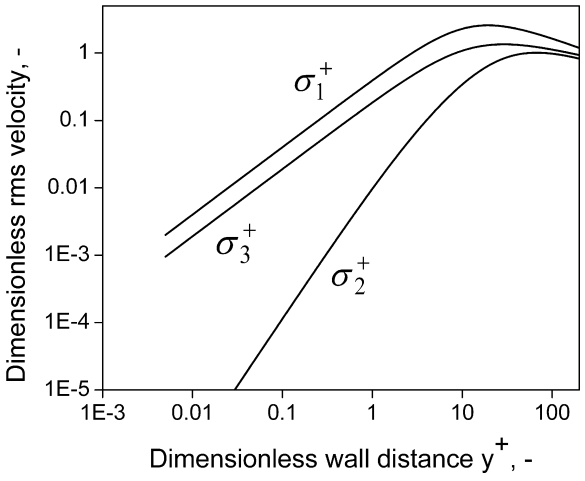

Fig. 1. rms of velocity components in the boundary layer.

Although these fits are not universal, they are found to be only slightly dependant on the Reynolds number for predominantly two dimensional flows (Antonia et al., 1992), and should therefore provide better results than the default CFD code model which typically assumes isotropic turbulence all the way to the wall. The rms values of velocity are plotted in Fig. 1. One clearly sees in particular that the wall normal fluctuations are very much smaller than the streamwise and spanwise components in the laminar sublayer.

The drift correction term in the streamwise direction (Eq. 21) in not readily available from the DNS literature. It is set here to zero, which should not alter the predictions significantly since it is the turbulent motion in the wall normal direction which controls the overall particle dispersion and deposition physics.

8. Application of the model in general geometries

Particle diffusion is usually studied in simple geometries such as parallel channels or pipes. To be of more practical interest, the current model is extended to handle arbitrary geometries in 3D. Mean flow data are supplied by CFD type codes with appropriate turbulence models. The procedure to use the Langevin equations to obtain the fluctuating velocities in general geometries is described next. In this procedure, it is assumed that the rms velocity values in complicated geometries can locally be approximated by the available DNS data for fully developed flows in simple channel geometry. While clearly an approximation, the latter assumption should provide a closer prediction of reality than taking turbulence to be isotropic throughout the domain.

The algorithm is schematically described by the flowchart in Fig. 2. At any time t during the trajectory integration, the particle distance to the nearest wall and its associated y^+ are computed. If the particle is inside the boundary layer, as in shown in Fig. 3 (in 2D for simplicity of illustration), a body fitted coordinate system (BFCS) is determined at the particle location based on the nearest wall face. In the BFCS, the streamwise unit vector is obtained by normalizing the local mean velocity vector at the particle location, while the normal unit vector is obtained from the vector normal to the nearest wall face. Finally, the spanwise unit vector is just the cross product of the abovementioned unit vectors. The rms of velocities are computed in the BFCS according to Eqs. (37)–(39), and one then computes in the BFCS the new fluctuating velocity vector at time ($t + \Delta t$) as specified by Eqs. (21)–(23).

Next, the fluctuating velocity components are transformed back to the computational coordinates system (CCS), and added to the mean velocities so that the particle tracking can be performed one additional time-step. This propels the particle to a new position at $t + \Delta t$ (see Fig. 3), with, depending on the cases, a new BFCS. The procedure described above is then repeated as long as necessary.

If the particle is in the bulk region, the Langevin equations for isotropic turbulence (Eqs. (28)–(30) are advanced in time directly in the CCS, and then the fluctuating values are added to the mean velocities to allow the trajectory calculations to be advanced one additional time step.

The computation for a particular particle continues until the particle is trapped by the wall or leaves the computational domain.

9. Implementation of the CRW model in the Fluent code

The Fluent CFD code (Fluent, 2006) provides the mean flow parameters as well as a facility to integrate the particle equations of motion. The stochastic model described in earlier sections was implemented in Fluent as a User Defined Function (UDF) subroutine which supplies the trajectory calculation module with the fluctuating fluid velocity seen by a particle at each time step. For

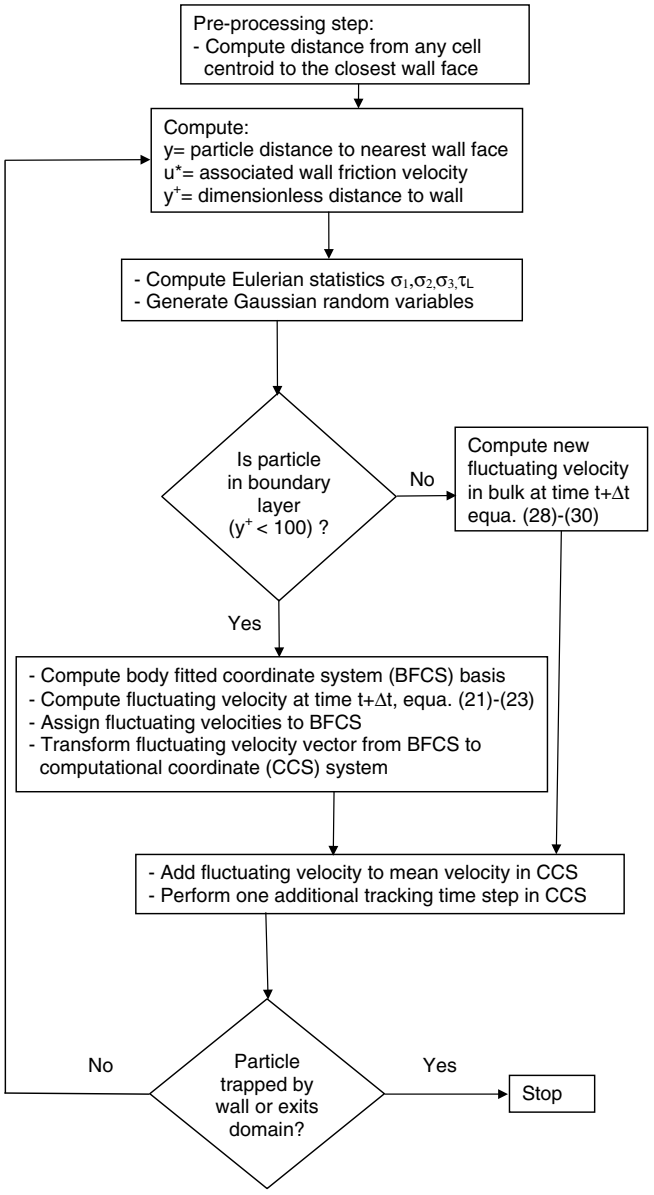

Fig. 2. Algorithm for Lagrangian particle tracking in general geometries.

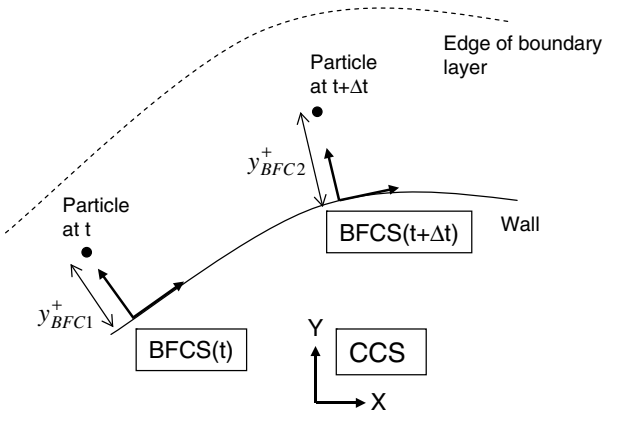

Fig. 3. Schematic of particle tracking in the boundary layer.

that purpose, a pre-processing step is necessary before performing the trajectory computation, and this consists in determining the wall face which has the shortest distance to the centroid of any cell in the domain (first step in flow chart Fig. 2). The latter calculation is performed just once for any converged solution, but it can sometimes be quite CPU intensive, especially for mesh sizes greater than 1 million.

10. Results and discussion

The CRW Langevin model just outlined was used to verify the well-mixed criterion, then extensive benchmarks were conducted against particle deposition data is simple pipe flows, 90° bends, and finally an idealized 3D geometry of a human mouth-throat.

10.1. Verification of the well-mixed criterion

One of the most stringent tests for any turbulent dispersion model is the so-called well-mixed criterion, that is, the requirement that very low inertia particles which are uniformly mixed in the domain should remain well mixed as time evolves. For this particular benchmark, a pipe flow with a Reynolds number equaling 10000 was chosen. The fluid is air at atmospheric conditions, and the pipe diameter and length are 0.01 m and 0.1 m, respectively, while the mean inlet velocity is 14.6 m/s. Periodic boundary conditions are imposed on the inlet and outlet of the pipe, hence ensuring a fully developed flow field. The CFD mesh consists of about 1 million hexahedral cells, and the centroid of the wall nearest cell has a y^+ of about 1. There are 20 cells within the boundary layer (y^+ <100), in accordance with the CFD Best Practice Guidelines for enhanced wall treatment (ERCOFTAC, 2000). The flow conditions are such that 2/3 of the cross sectional area is in the boundary layer, whereas the remaining 1/3 is in the bulk region.

The turbulence model used is the standard k–ε. After the second order accurate mean flow solution is converged, 10000 tracer spherical particles with diameter 0.7 μm and unit density are uniformly injected with the mean fluid velocity at the entrance face. The particles have a dimensionless relaxation time τ_p^+ of 0.11 where

$$\tau_p^+ = \frac{\tau_p u*^2}{\nu} \tag{40}$$

Particles which reach the pipe outlet are re-injected from the inlet with their latest velocity values, in compliance with the periodic boundary conditions. The distribution of particles at later times is determined as follows: the volume of the pipe is subdivided in 10 concentric annuli with equal volumes, then, at a given time t^+, the number of particles in each annulus is counted, and the concentration profile is obtained by normalizing the number of particles in each bin with the total number of particles in the domain. On impact with the wall, particles are reflected. In a first computation, the drift correction in the Langevin equations is not considered. In Fig. 4, the particle distribution is displayed for times t^+ = 3, and 10, where t^+ = 1 corresponds to the mean time required by a fluid particle to travel across the pipe length. One clearly sees a non-physical concentration build-up in the boundary layer, known as the "spurious drift" (MacInnes and Bracco, 1992). This build-up also gets worse with time and many impacts with the wall are recorded. In contrast, when the drift correction is used, the particles are roughly uniformly distributed in the domain as shown in Fig. 5, and this result is holds at long times. In addition, the number of impacts with the wall is virtually zero. The slight peak at a z/R of about 0.3 coincides with the transition between the boundary layer and the bulk flow, and may be due to the discontinuity between the time scales in the two regions at y^+ of 100. Still, the normalized concentrations have a mean deviation from the ideal result of only 13 %, and hence, the well-mixed crite-

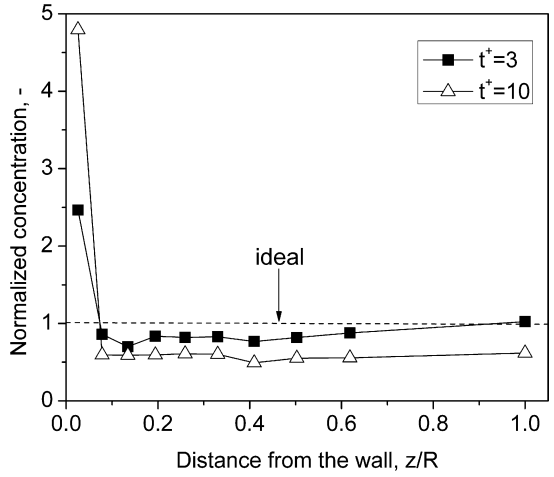

Fig. 4. Normalized concentration of tracer particles. No drift correction.

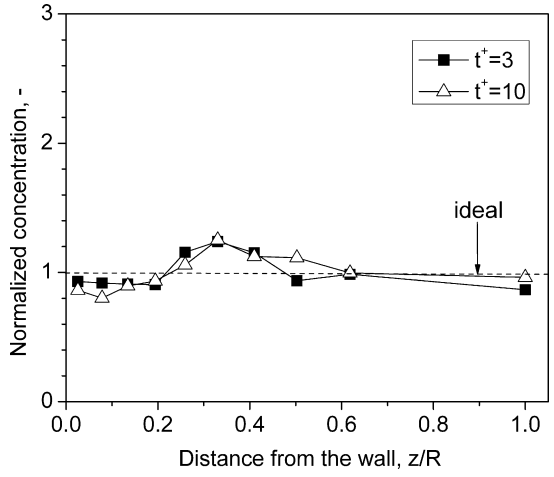

Fig. 5. Normalized concentration of tracer particles. With drift correction.

rion is met with a good degree of accuracy. These results show that it is very important to include the drift corrections to avoid erroneous predictions for low-inertia particle dispersion.

10.2. Turbulent deposition in pipe flow

The deposition of particles in turbulent vertical pipe flows has been experimentally studied by a number of authors. McCoy and Hanratty (1977) gathered a large database from various investigations and proposed the following best fit for the dimensionless deposition velocity V^+ as a function of the dimensionless relaxation time τ_p^+:

$$V^+ = 0.000325 \cdot \tau_p^{+2}, \quad 0.2 \leqslant \tau_p^+ \leqslant 22.9 \tag{41}$$

$$V^+ = 0.17, \quad \tau_p^+ > 22.9 \tag{42}$$

where the dimensionless deposition velocity for a pipe of diameter D and length L is defined as

$$V^+ = \frac{1}{4}\frac{D}{L}\frac{\overline{U}}{u^*}\ln\left(\frac{C_{in}}{C_{out}}\right) \tag{43}$$

D and L are the pipe diameter and length, respectively, while the C's refer to particle number concentrations.

A CFD grid was prepared based on the geometry and test conditions of the well known experiments by Liu and Agarwal (1974). The latter authors measured the deposition of 1.4–21 μm diameter

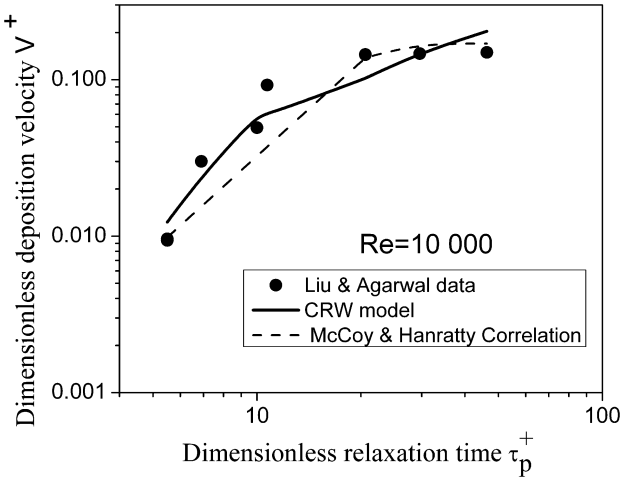

Fig. 6. Comparison for pipe deposition velocity at $Re = 10\,000$.

olive oil particles injected in a vertical glass pipe of diameter 1.27 cm and length 1 m. Deposition data is presented for the portion of the pipe section between 0.255 m and 0.763 m (0.508 m), i.e. in the region where the flow is fully developed and far enough from the outlet. Two sets of mean gas velocities are used, that is 12 m/s and 62 m/s, which correspond to Reynolds numbers of approximately 10000 and 50000, respectively.

In the CFD simulation, two sets of 3D hexahedral meshes are generated for the two Reynolds number cases. For this simple flow case, the standard k–ε turbulence model is used, along with enhanced wall treatment. The near-wall cell has a y^+ less than 1, and there are about 30 cells inside the boundary layer, so the latter is very well resolved. Once the second order accurate CFD solution is reached, the CRW Lagrangian tracking is performed by following the paths of 10000 spherical particles of density 920 kg/m^3 uniformly distributed over the inlet face. The particles are assigned the gas velocity at the time of release. The chosen number of particles of 10000 is adequate, as preliminary simulations with larger numbers of particles showed no change in the deposition rate beyond 5000 particles. A particle is considered deposited when its center of mass is located less than one particle radius from the nearest wall.

The particle deposition results are shown in Figs. 6 and 7 for the two Reynolds numbers of 10000 and 50000, respectively. The CRW model predicts quite well both the trends and the magnitude of

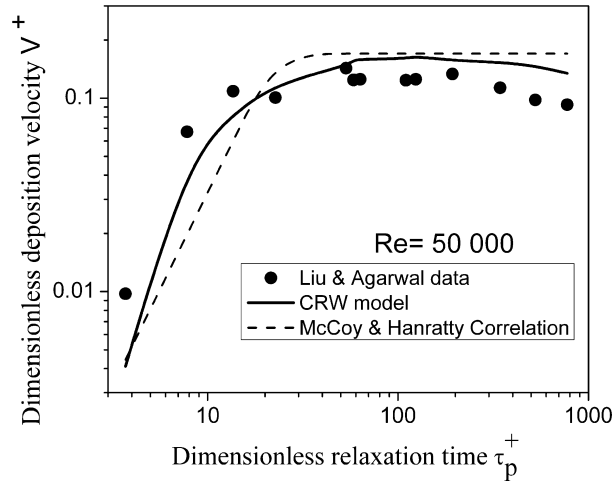

Fig. 7. Comparison for pipe deposition velocity at $Re = 50\,000$.

deposition. In general, the CRW deposition rates lie between those of the McCoy and Hanratty fits and the Liu and Agarwal data.

It should to be noted that the spatial resolution for LPT needs to be significantly finer than what is required to obtain grid independent results for the flow field. For instance, a mesh with 0.5 million cells was adequate to produce a grid-independent flow field for both cases. However, it was necessary to have about 4.4 million cells for $Re = 10000$ and 6.0 million cells for $Re = 50000$ to reach grid-independent results for particle deposition. This is directly related to two facts: firstly, LPT calculations involve heavy interpolations, as particles almost never coincide with the grid locations, and secondly, the grid resolution at the curved wall should be fine enough that the smallest particles "see" no kinks at the junction between two neighboring wall faces, otherwise, they may artificially deposit when they should not necessarily do so had the neighboring wall surfaces been smoothly connected.

10.3. Turbulent deposition in 90° bends

Experimental studies of deposition in bends have largely concentrated on laminar flow. To the best of the author's knowledge, the only two published experimental works performed in turbulent conditions are due to Pui et al. (1987) and McFarland et al. (1997) who measured the penetration of particles through bends with diameters on the order of 1–2 cm. Both experiments predict similar deposition rates, so we restrict ourselves here to the work of Pui et al. (1987) who provided the following correlation for the best fit through their data:

$$\phi = 1 - \frac{C_{\text{out}}}{C_{\text{in}}} = 1 - \exp(-2.823 \cdot Stk \cdot \theta) \tag{44}$$

where ϕ is the deposited fraction, the C's the inlet and outlet aerosol concentrations, respectively, θ the bend angle in radians, and Stk the particle Stokes number defined as

$$Stk = \frac{\tau_p \overline{U}}{D} \tag{45}$$

in which $\overline{U}$ is the mean gas velocity in the pipe, D is the pipe diameter, and τ_p the particle relaxation time defined earlier. No specific uncertainty is given, but the data is enveloped by the correlation within a 30% band. The bend represents an interesting geometry, because unlike what happens in a straight pipe, deposition on a bend is caused by two processes instead of one, namely inertial impaction, which is dominant and turbulent dispersion, which is an enhancement mechanism.

A generic 90° bend section with 2 cm diameter and radius of curvature 4.0 is modeled The domain includes a straight inlet pipe with a 5 D developing length as well as an outlet straight section with 5 D length. A 3.0 m/s velocity boundary condition ($Re = 4080$) is imposed at the inlet, and a 0 gauge pressure is imposed at the outlet. The hexahedral mesh has 0.8 million cells and is fine enough to resolve the boundary layer and produce grid independent results for the particle tracking. The Reynolds Stress Model (RSM) is used for modeling the mean turbulence, along with enhanced wall treatment and second order accuracy. Particle tracking is conducted by releasing 10000 uniformly distributed unit density particles from the entrance face of the bend. Particle deposition is recorded for the bend as well as the outlet straight section, because the effect of the bend is felt beyond the bend itself. Moreover, the McCoy & Hanratty correlation (1977) shows that for the conditions of this simulation, no deposition will take place on the 5 D outlet straight section in the absence of the bend. Hence the deposition in the entire domain can be solely attributed to the presence of the bend.

Comparison between the correlation and both the CRW and "mean tracking" model is shown in Fig. 8. Mean flow tracking involves using the mean flow velocities from the CFD solver without adding the contribution of turbulence. As can be seen, the agreement between the data and the CRW model is excellent across the range of particle inertia. The mean flow tracking shows good agreement with the Pui correlation for low and high inertia particles. This is expected, since low and high inertia particles are only slightly affected by turbulence. For mid-range inertia particles, the turbulent fluctuations are responsible for enhanced particle deposition, and this is very well predicted only by the CRW model.

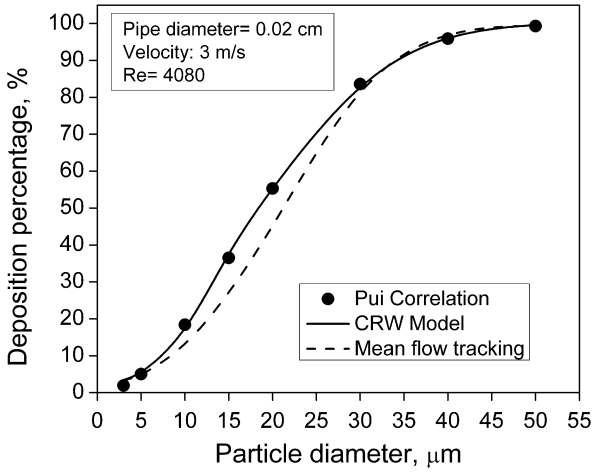

Fig. 8. Comparison for 90° bend deposition at $Re = 4080$.

10.4. Turbulent deposition in 3D mouth-throat geometry

There is only scarce data relating to particle deposition in complex three dimensional turbulent flows. Among the available data is information relative to medical aerosol removal rates in the human extrathoracic region encompassing the mouth, the pharynx, the larynx and the trachea. Aerosol deposition in those regions is unwelcome because the medication is meant for the lungs which are located further downstream. Good quality, albeit limited data was recently provided by Grgic et al. (2004) who measured the removal of 3, 5 and 6.5 μm DEHS oil particles (density 912 kg/m^3) in an idealized mouth-throat geometry (Fig. 9). The latter was constructed from tomographic scans of many adult patients with no apparent abnormalities (DeHaan and Finlay, 2001). Grgic et al. (2004) used two distinct flow rates, i.e. 30 and 90 l/min. For 30 l/min, the flow is transitional to slightly turbulent, with a Reynolds number on the order of 2700 based on the entrance pipe diameter of 17 mm. For 90 l/min, the flow is turbulent, and the Reynolds number is of the order of 8000.

Because of the complicated 3D geometry, a hybrid CFD mesh is used. This consists of four prism layers near the wall, a tetrahedral mesh in the bulk, and a pyramid mesh layer in the transition region. The original mesh has 1.1 millions cells in order to resolve the boundary layer such that the RSM model with enhanced wall treatment can be used. For these conditions, it is required that the wall-nearest cell centroid have a y^+ of order 1. A second mesh having 3.3 million cells is generated in order to ensure that the results are grid-independent. Both meshes gave virtually identical results for the particle deposition. A flat velocity profile is imposed on the inlet face of a short 17 mm diameter pipe which provides a fully developed flow into the mouth-throat section. A 0 gauge pressure is imposed on the outlet face.

Once the second order accurate mean flow solution is converged, 10000 particles are injected uniformly at the entrance face, and the recorded deposition fractions are as shown in Table 1 for a flow rate of 90 lpm. These are compared with the Grgic et al. (2004)

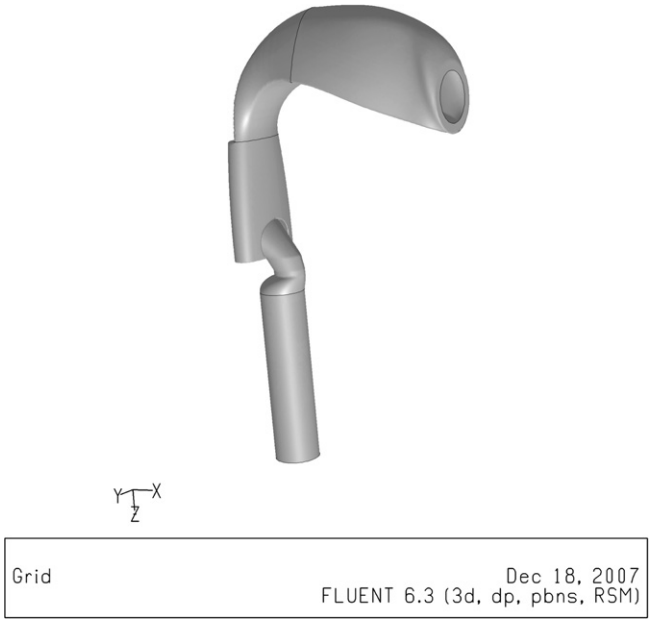

Fig. 9. Schematic of the Alberta mouth-throat geometry.

Table 1
Deposition fraction (%) in the mouth-throat geometry at a flowrate of 90 lpm

Particle diameter (μm)	Data by Grgic et al.	CRW model	Mean flow tracking
3.0	33 ± 5	23.4	4.0
5.0	68 ± 3	59.5	17.2
6.5	78 ± 3	80.1	33.0

data as well as the mean flow tracking results. The deposition predictions of the CRW model are in quite good agreement with the data. In contrast, the mean flow tracking underpredicts the deposition rate significantly, as the enhancing effects of turbulence are not taken into account.

Grgic et al. (2004) found that their data at a flow rate of 90 lpm was in close agreement with the best fit by Stahlhofen et al. (1989). The latter had produced their fit from a large number of experimental investigations, and displayed the deposition fraction as a function of the particle inertial parameter $\rho_p d_p^2 Q$, where Q is the volumetric flow rate. The model predictions at 90 lpm were subsequently compared to the Stahlhofen fit for a wide range of particle diameters as shown in Fig. 10. As can be seen, the agreement between the model and the Stahlhofen fit is very good over the whole range of particle inertia.

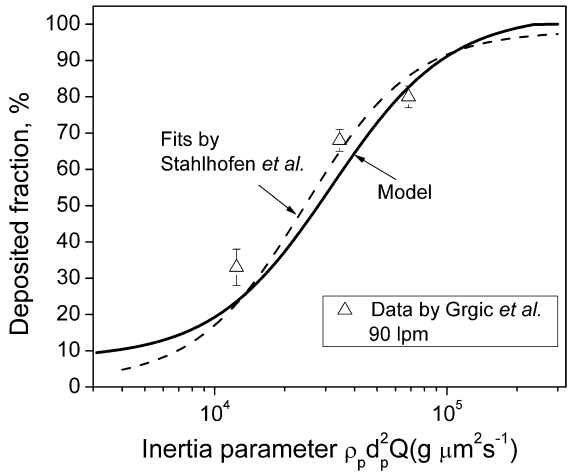

Fig. 10. Model prediction versus Stahlhofen correlation.

Table 2
Deposition fraction (%) in the mouth-throat geometry at a flowrate of 30 lpm

Particle diameter (μm)	Data by Grgic et al.	CRW model	Mean flow tracking
3.0	2 ± 2	6.4	4.4
5.0	11 ± 3	11.8	4.1
6.5	32 ± 3	21.6	5.8

In a second simulation, the model was compared with the Grgic et al. (2004) data at a flow rate of 30 lpm. The results are shown in Table 2. Again, the prediction of the CRW compare favorably with the data, whereas the mean flow tracking largely underpredicts the deposition rate.

11. Conclusions

A Lagrangian continuous random walk (CRW) model is developed to predict particle dispersion in arbitrary wall-bounded geometries with prevailing anisotropic, inhomogeneous turbulence. The particle tracking model relies on 3D mean flow data provided by the Fluent CFD code, as well as Eulerian statistics computed from DNS databases. The time history of the fluctuating fluid velocities is obtained from the normalized Langevin equation which takes into account turbulence inhomogeneities. The model incorporates a drift velocity correction for arbitrary inertia particles. Using this correction, it is shown that tracer particles remain largely well-mixed if introduced uniformly in the domain. Benchmarks of the model are performed against particle deposition data in simple turbulent pipe flows, 90° bends, as well as more complex 3D flows inside an idealized mouth-throat geometry. Good agreement with the data is obtained across the range of particle inertia. Overall, it is shown that Lagrangian CRW, coupled with DNS Eulerian statistics and CFD mean flow data, is able to properly predict the main features of turbulent particle dispersion in general geometries with inhomogeneous turbulence. This pleads in favor of incorporating such enhanced CRW models in CFD codes to accurately describe turbulent particle dispersion in general geometries.

Acknowledgements

The author wishes to express his gratitude to Dr. W. Timm of Fluent Deutschland GmbH, for extensive interactions during this work. Special thanks are also due to Professor W. Finlay of the University of Alberta for making available the CAD files of the Alberta mouth-throat geometry and to Professor E. Loth of the University of Illinois for useful discussions.

References

Antonia, R.A., Teitel, M., Kim, J., Browne, L.W.B., 1992. Low-Reynolds-number effects in a fully developed turbulent channel flow. J. Fluid Mech. 236, 579–605.
Bocksell, T.L., Loth, E., 2001. Random walk models for particle diffusion in free shear flows. AIAA J. 39, 1086–1096.
Bocksell, T.L., Loth, E., 2006. Stochastic modeling of particle diffusion in a turbulent boundary layer. Int. J. Multiphase Flow 32, 1234–1253.
DeHaan, W.H., Finlay, W.H., 2001. In Vitro monodisperse aerosol deposition in a mouth and throat with six different inhalation devices. J. Aerosol Med. 14, 361–367.
Dehbi, A., 2008. A CFD model for particle dispersion in turbulent boundary layer flows. Nucl. Eng. Des. 238, 707–715.
Dreeben, T.D., Pope, S.B., 1997. Probability density function and Reynolds-stress modeling of near-wall turbulent flows. Phys. Fluids 9, 154–163.
Drew, D.A., 1983. Mathematical modeling of two-phase flow. Ann. Rev. Fluid Mech. 15, 261–291.
Durbin, P.A., 1983. Stochastic differential equations and turbulent dispersion, NASA Reference Publication 1103.
Durbin, P.A.,1984. Comments on the papers by Wilson et al. (1981) and Legg and Raupach (1982). Bound. Layer Meteorol. 29, 409–411.

ERCOFTAC, 2000. European Research Community on Flow Turbulence and Combustion (ERCOFTAC) Best Practice Guidelines, Version 1.
Fluent, 2006. Fluent 6.3 Users Guide, Lebanon, USA.
Gosman, A.D., Ioannides, E., 1983. Aspects of computer simulation of liquid fuelled combustors. J. Energy 7, 482–490.
Grgic, B., Finlay, W.H., Heenan, A.F., 2004. Regional aerosol deposition and flow measurements in an idealized mouth and throat. J. Aerosol Sci. 35, 21–32.
Healy, D.P., Young, J.B., 2001. Calculation of inertial particle transport using the Osiptsov Lagrangian method. In: 4th International Conference on Multiphase Flow, New Orleans, Paper DJ4.
Iliopoulos, I., Hanratty, T.J., 1999. Turbulent dispersion in a non-homogeneous field. J. Fluid Mech. 293, 45–71.
Iliopoulos, I., Mito, Y., Hanratty, T.J., 2003. A stochastic model for solid particle dispersion in a nonhomogeneous turbulent field. Int. J. Multiphase Flow 29, 375–394.
Kallio, G.A., Reeks, M.W., 1989. A numerical simulation of particle deposition in turbulent boundary layers. Int. J. Multiphase Flow 3, 433–446.
Kröger, C., Drossinos, Y., 2000. A random-walk simulation of thermophoretic particle deposition in a turbulent boundary layer. Int. J. Multiphase Flow 26, 1325–1350.
Legg, B.J., Raupach, M.R., 1982. Markov-chain simulation of particle dispersion in inhomogeneous flows: The mean drift velocity induced by a gradient in Eulerian velocity variance. Bound. Layer Meteorol. 24, 3–13.
Liu, B.Y.H., Agarwal, J.K., 1974. Experimental observation of aerosol deposition in turbulent flow. Aerosol Sci. 5, 145–155.
MacInnes, J.M., Bracco, F.V., 1992. Stochastic particle dispersion modeling and the tracer particle limit. Phys. Fluids A 4, 2809–2824.
Marchioli, C., Soldati, A., 2002. Mechanisms for particle transfer and segregation in turbulent boundary layer. J. Fluid Mech. 468, 283–315.
Maxey, M.R., 1987. The motion of small spherical particles in a cellular flow field. Phys. Fluids 30, 1915–1928.
McCoy, D.D., Hanratty, T.J., 1977. Rate of deposition of droplets in annular two-phase flow. Int. J. Multiphase Flow 3, 319–331.
McFarland, A.R., Gong, H., Muyshondt, A., Wente, W.B., Anand, N.K., 1997. Aerosol deposition in bends with turbulent flow. Environ. Sci. Technol. 31, 3371–3377.
McLaughlin, J.B., 1989. Aerosol particle deposition in numerically simulated channel flow. Phys. Fluids A 1, 1211–1224.
Mito, Y., Hanratty, T.J., 2002. Use of a modified Langevin equation to describe turbulent dispersion of fluid particles in a channel flow. Flow, Turbul. Combust. 68, 1–26.
Mito, Y., Hanratty, T.J., 2004. A stochastic description of wall sources in a turbulent field: part 2. Calculation for a simplified model of horizontal annular flows. Int. J. Multiphase Flow 30, 803–825.
Obukhov, A.M., 1959. Description of turbulence in terms of Lagrangian variables. Adv. Geophys., 113–116.
Parker S., Foat, T., Preston, T., 2007. Towards quantitative prediction of aerosol deposition from turbulent flows. J. Aerosol Sci., doi: 10.1016/j.jaerosci.2007.10.002.
Perkins, R.J., 1992. The entrainment of heavy particles into a plane turbulent jet. In: Proceedings of the 6th Workshop on Two-phase Flow Predictions, Erlangen, ed. M. Sommerfeld, pp. 18–33.
Pozorski, J., Minier, J.P., 1998. On the Lagrangian turbulent dispersion models based on the Langevin equation. Int. J. Multiphase Flow 24, 913–945.
Pui, D.Y.H., Romay-Novas, F., Liu, B.Y.H., 1987. Experimental study of particle deposition in bends of circular cross section. Aerosol Sci. Technol. 7, 301–315.
Stahlhofen, W., Rudolf, G., James, A.C., 1989. Intercomparison of experimental regional aerosol deposition data. J. Aerosol Med. 2, 285–308.
Squires, K.D., Eaton, J.K., 1991. Measurements of particle dispersion obtained from direct numerical simulations of isotropic turbulence. J. Fluid Mech. 226, 1–35.
Thompson, D.J., 1984. Random walk modeling of dispersion in inhomogeneous turbulence. Quart. J. Roy. Meteorol. Soc. 110, 1107–1120.
Thompson, D.J., 1987. Criteria for the selection of stochastic models of particle trajectories in turbulent flows. J. Fluid Mech. 180, 529–559.
Tian, L., Ahmadi, G., 2007. Particle deposition in turbulent duct flow- Comparison of different model predictions. J. Aerosol Sci. 38, 377–397.
Wang, Q., Squires, K.D., 1997. Large eddy simulation of particle deposition in a vertical turbulent channel flow. Int. J. Multiphase Flow 22, 667–683.
Wilson, J.D., Thurtell, G.W., Kidd, G.E., 1981. Numerical simulation of particle trajectories in inhomogeneous turbulence. Part 2: Systems with variable turbulent velocity scale. Bound. Layer Meteorol. 21, 423–441.
Yeung, P.K., Pope, S.B., 1989. Lagrangian statistics from direct numerical simulations of isotropic turbulence. J. Fluid Mech. 207, 531–586.
Zhang, D.Z., Prosperetti, A., 1994. Averaged equations for inviscid disperse two phase flows. J. Fluid Mech. 267, 185–219.